Supporting Information

Improved Bi-Layer Electrolytes of Solid Oxide Cells: The Role of $Sm_{0.2}Ce_{0.8}O_{2-\delta}$ Diffusion Barrier Layer

Su-Wan Kim †, Hae-In Jeong †, Dong-Yeon Kim, Beom-Kyeong Park *

Department of Materials Science and Engineering, Pusan National University, Busandaehak-ro 63beon-gil 2, Geumjeong-gu, Busan 46241, Republic of Korea

*** Corresponding author**

E-mail: b-park@pusan.ac.kr

† These authors contributed equally.

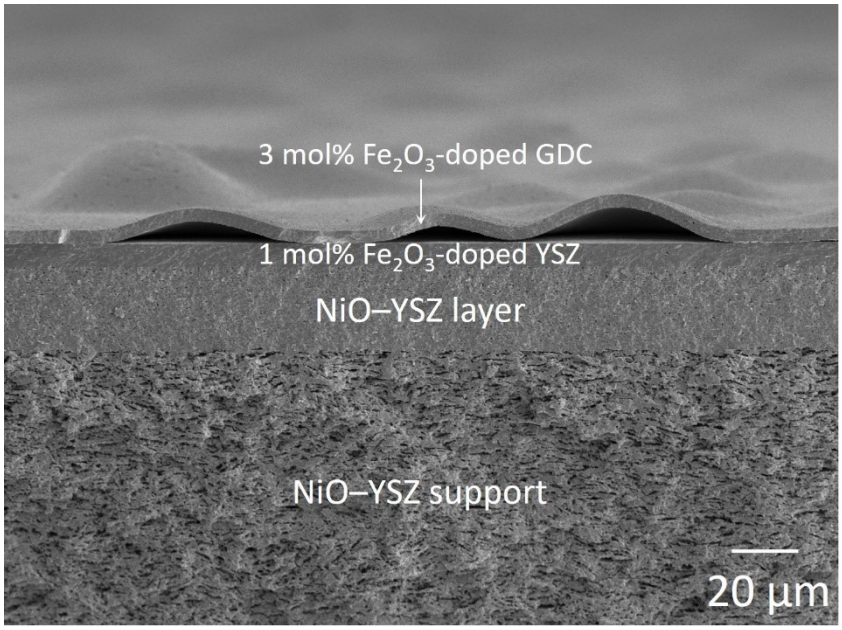

Fig. S1. Cross-sectional SEM image of a NiO–YSZ supported half-cell with 3 mol% Fe_2O_3-doped GDC layer, fabricated through a single step 1250 ^oC sintering.

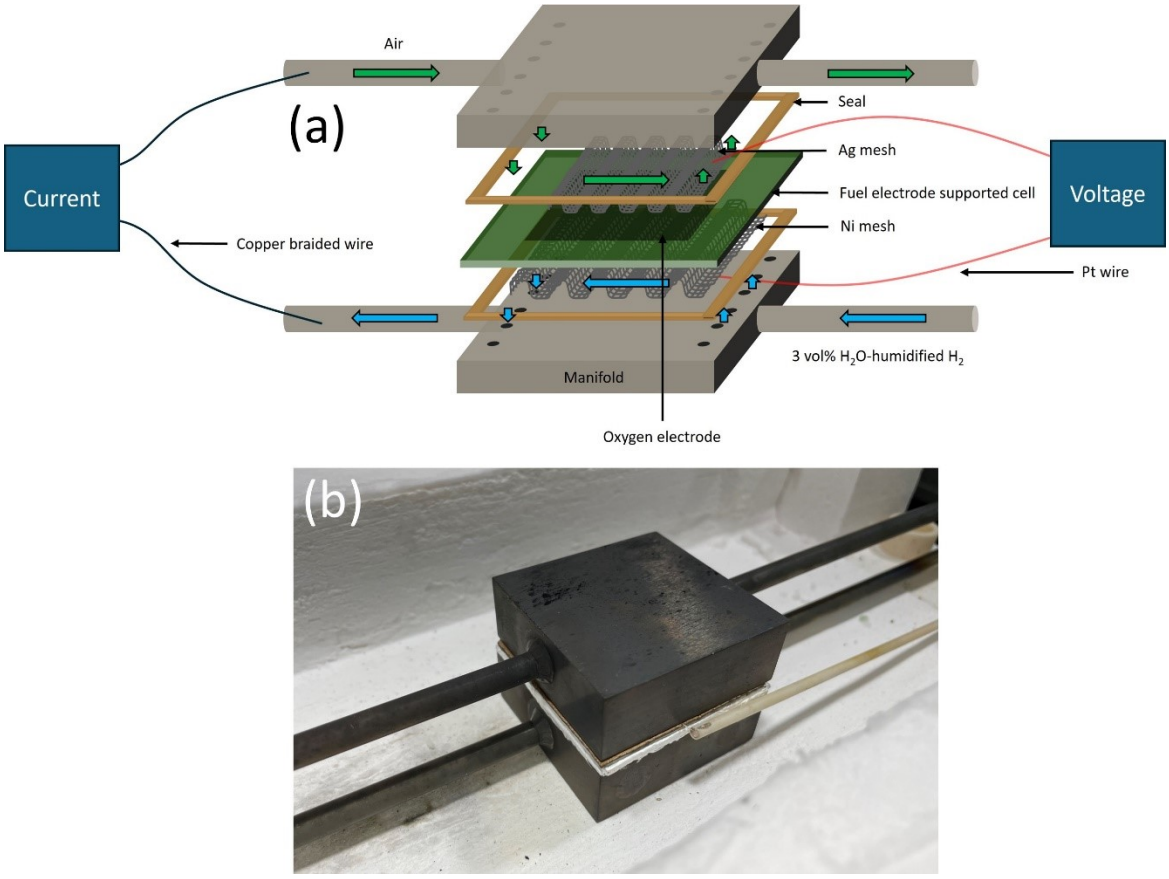

Fig. S2. **(**a) Schematic and (b) photograph of the cell assembly with manifolds used for testing a large area (~22.09 cm^2) Ni–YSZ FESC.

A large area (~22.09 cm^2) Ni–YSZ FESC with a YSZ/SDC:F1 electrolyte and a 9 cm^2 LSCF–GDC oxygen electrode was tested as proof-of-concept, using a commercial 5 × 5 cm test fixture kit (fuelcellmaterials). To facilitate current collection, a silver grid (Heraeus, C4400UF) was screen-printed onto the LSCF–GDC electrode. An Ag mesh brush coated with LSM ink (or a Ni mesh brush coated with Ni ink) was applied to the oxygen electrode (or fuel electrode) for ensuring solid electrical contact between the full cell and the manifolds, before the cell was sandwiched between the manifolds. Pt wires were connected to each mesh as voltage probes. The assembly was sealed by placing a gasket around all edges of the manifold

and applying a compression force of 2.3 PSI. Fig. S2 presents a schematic overview of the cell assembly for testing, along with a photograph of the actual setup. The cell assembly was heated to 800 ^{o}C at a ramp rate of 2 °C min^{-1}, with air (800 sccm) flowing to the oxygen electrode and Ar (300 sccm) to the fuel electrode. The Ar flow was then switched to 3 vol% H_2O-humidified H_2 for the NiO reduction. Impedance spectra were obtained at temperatures ranging from 600 to 700 ^{o}C.

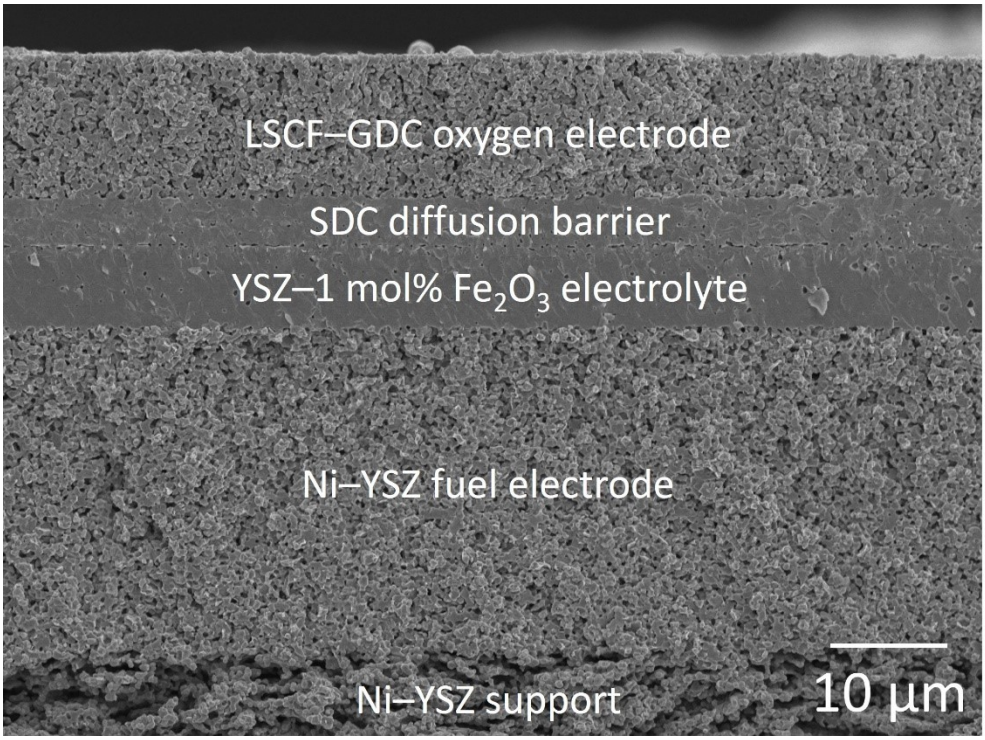

Fig. S3. Cross-sectional SEM image of a Ni–YSZ FESC with YSZ/SDC bi-layer electrolyte after electrochemical testing.

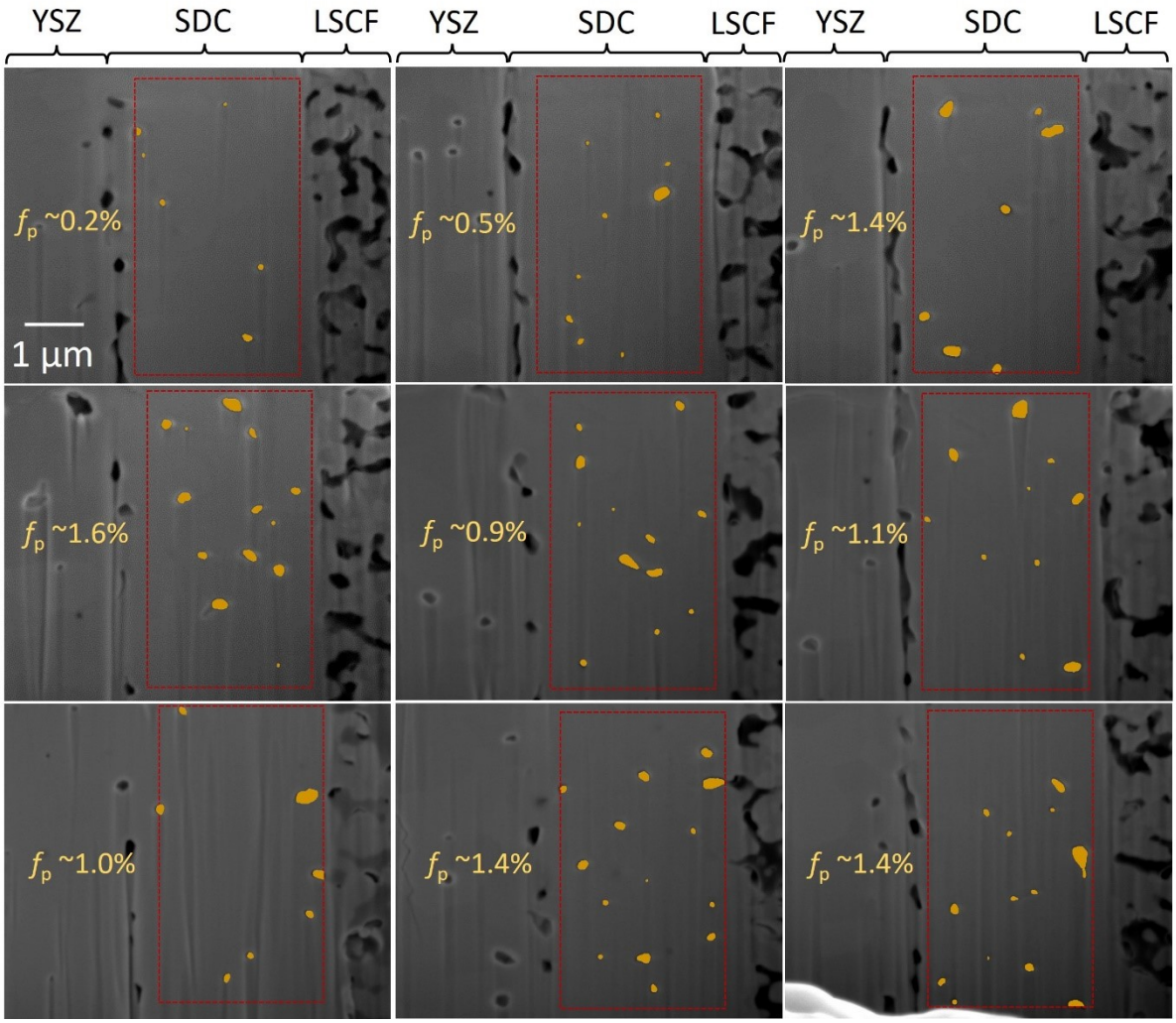

Fig. S4. FIB–SEM images showcasing various regions of the SDC electrolyte along with adjacent LSCF–GDC and YSZ layers. These images were processes using ImageJ software to apply a thresholding technique. The yellow-colored areas indicate residual pores, and f_p denotes the pore fraction.

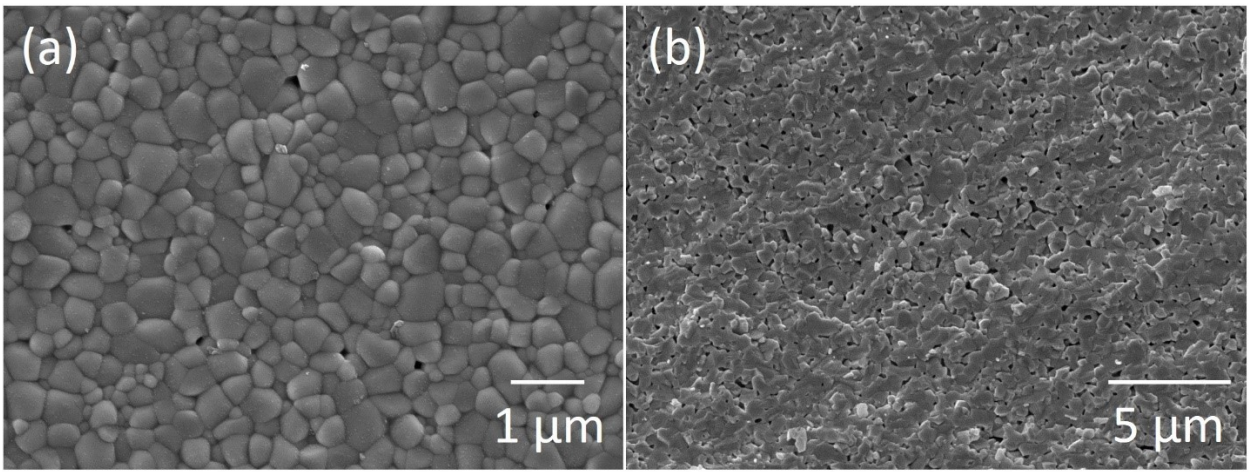

Fig. S5. (a) Surface and (b) cross-section SEM images of bulk SDC specimen prepared by tape casting.

Seven ~500 µm thick SDC substrates were fabricated via tape casting and lamination, as described in Section 2.1. The laminates were sintered at 1250 ^{o}C for 4 h. The average value of SDC relative density, measured using the Archimedes method, was determined to be~92.5 %, with a standard deviation of ~0.8.

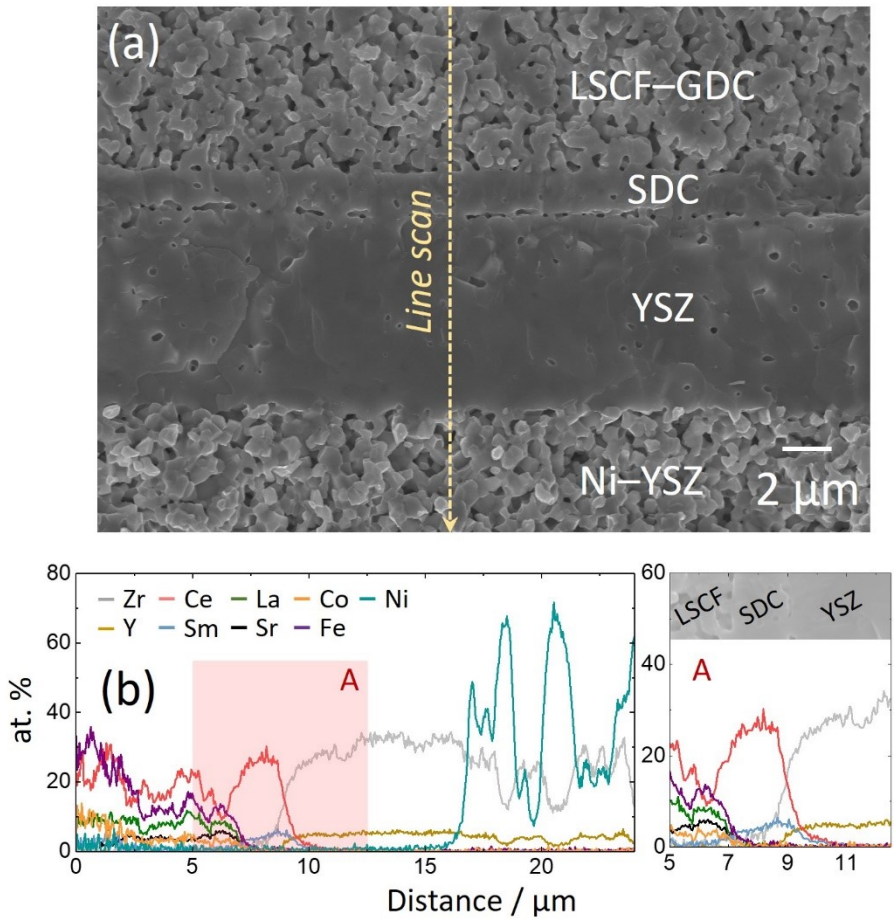

Fig. S6. (a) Fracture cross-sectional SEM image of the tested Ni–YSZ FESC with an ~1.5 µm-thick SDC diffusion barrier layer. (b) SEM–EDS line scan illustrating the elemental distribution across the SDC layer.

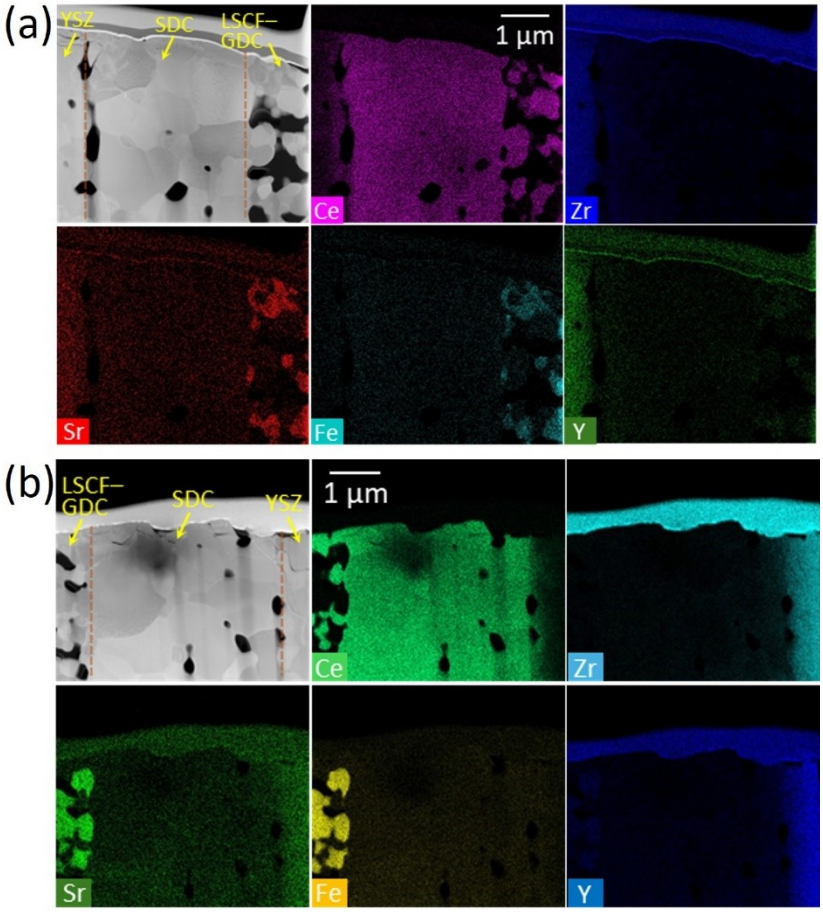

Fig. S7. STEM–EDS elemental maps for the SDC layer and the adjacent LSCF–GDC and YSZ layers, across two different regions of the tested Ni–YSZ FESC.

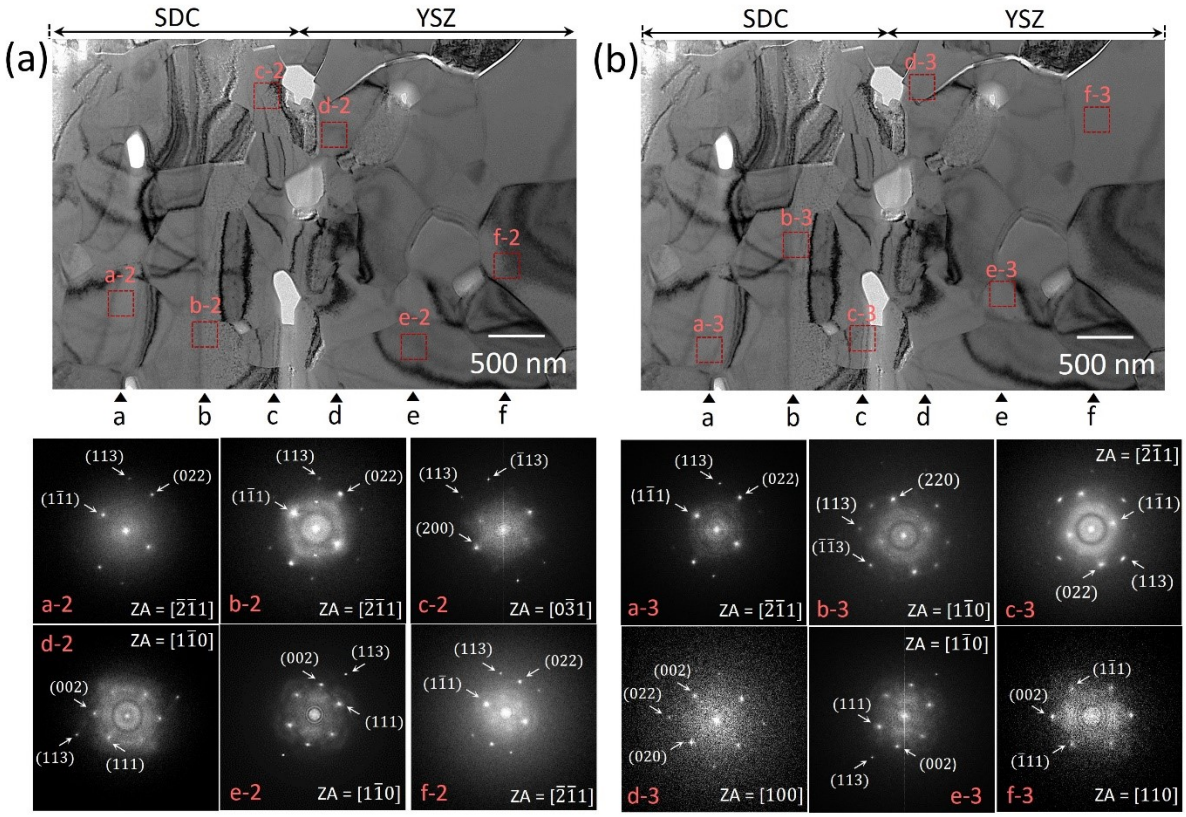

Fig. S8. Fast Fourier Transforms (FFTs) of the areas marked by red squares in the HRTEM image, showing the region near the YSZ/SDC interface in the tested Ni–YSZ FESC.

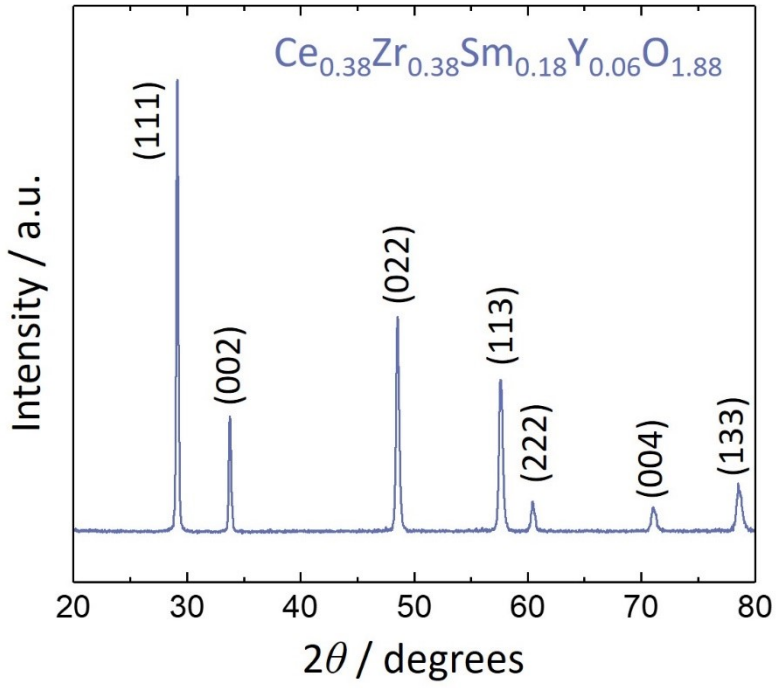

Fig. S9. XRD pattern of a $Ce_{0.38}Zr_{0.38}Sm_{0.18}Y_{0.06}O_{1.88}$ bulk specimen, which was sintered at 1400 °C for 5 h.

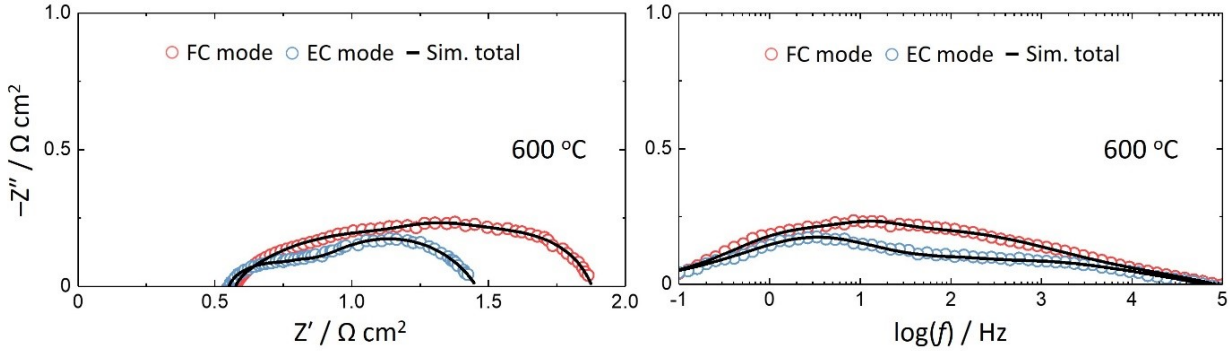

Fig. S10. 600 °C impedance spectra in Nyquist and Bode plots for the Ni–YSZ FESC with YSZ/SDC bi-layer electrolyte.

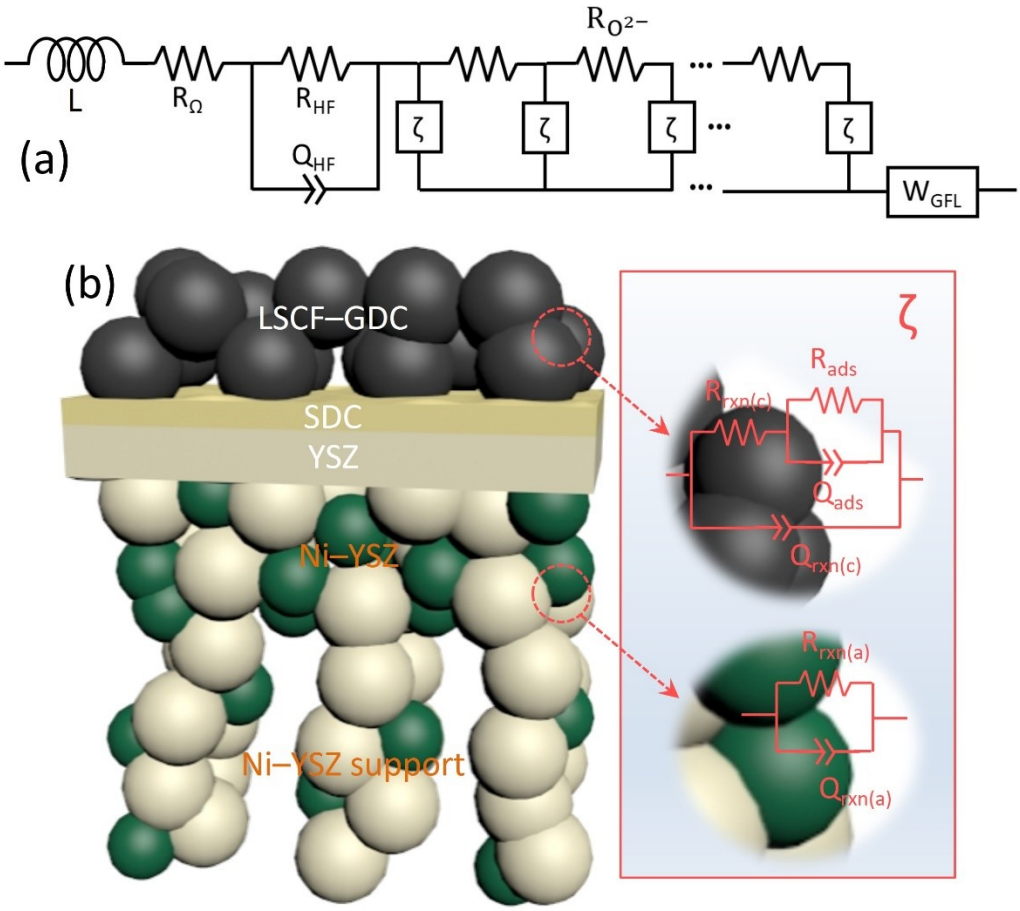

Fig. S11. (a) Equivalent circuit model (ECM) used to fit the EIS data of the Ni–YSZ FESCs. The ECM is composed of a transmission line model (TLM) which includes an interfacial element ς, better described in the schematic representation in (b).

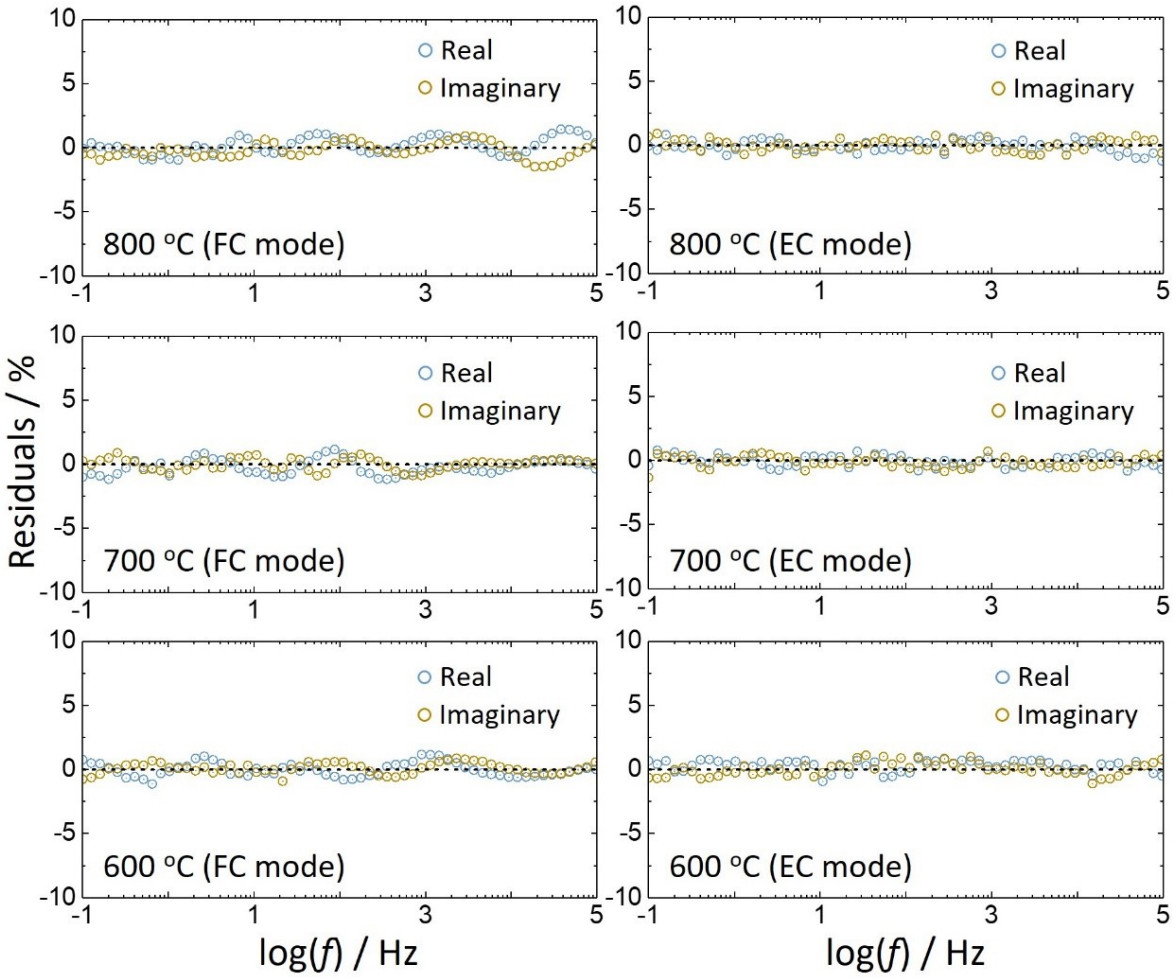

Fig. S12. Relative residuals between the measured EIS data and the model fits for the full Ni–YSZ FESC under fuel cell (3 vol% H_2O-humidified H_2 and air) and steam electrolysis (50 vol% H_2O-humidified H_2 and air) conditions.

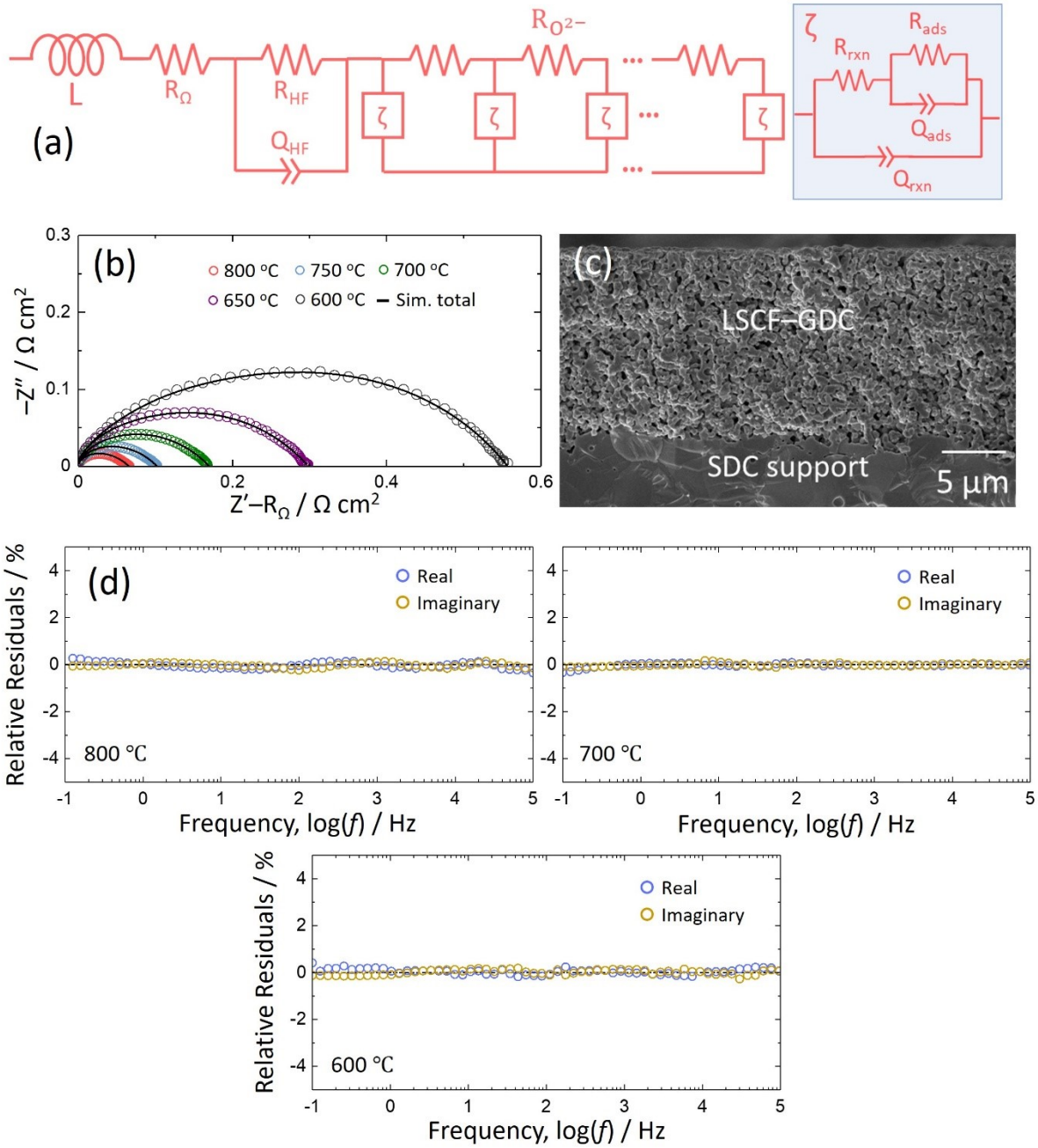

Fig. S13. (a) Equivalent circuit model (ECM) used to fit the EIS data of LSCF–GDC electrode symmetric cell. (b) Nyquist plots of the EIS data for LSCF–GDC cell measured at 600–800 °C in air, with fits the model shown in (a). (c) Cross-sectional SEM image of the LSCF–GDC after testing. (d) Relative residuals between the EIS data and the fits, confirming the good fitting.

The EIS fitting was done using an ECM in Figure S13(a), aimed at enabling more accurate estimations of the ohmic resistance R_{Ω} and electrode polarization resistance R_{P}. The model used here, previously developed for the LSCF electrode symmetric cell [1–4], includes a simplified transmission line, where R_{ion}, R_{rxn}, R_{ads} elements stand for oxygen conduction, surface exchange, dissociative adsorption/desorption. R_{Ω} is a resistor modeling the ionic resistance of the SDC support, while R_{HF} may be associated with the oxygen transfer between the GDC and LSCF interface. Lastly, L is added to account for inductive effects originating from the measurement circuit. The residuals, illustrated in Figure S13(d), all fall below ~1 %, indicating a good quality of fit.

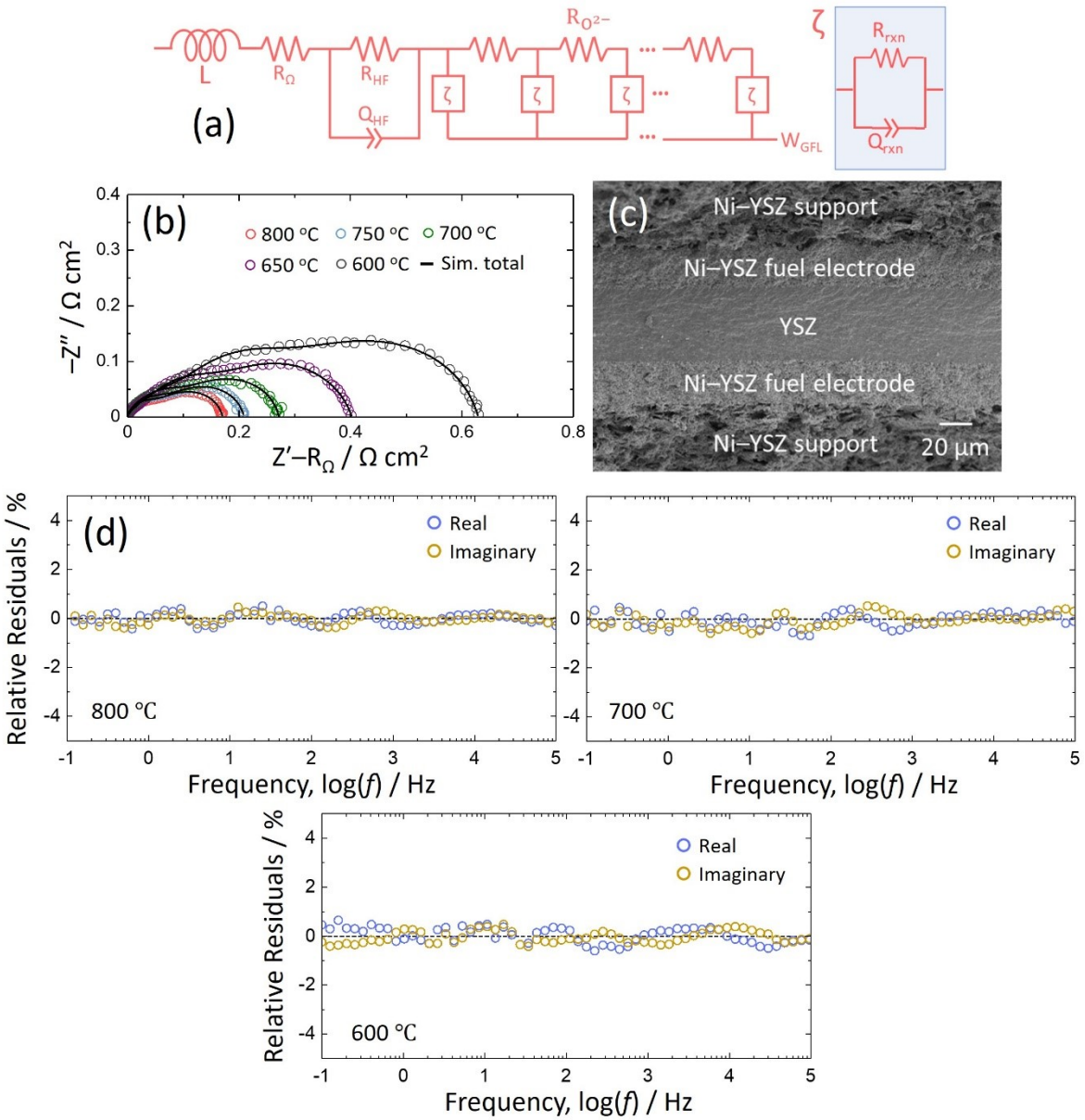

Fig. S14. (a) Equivalent circuit model (ECM) used to fit the EIS data of Ni–YSZ electrode symmetric cell. (b) Nyquist plots of the EIS data for Ni–YSZ cell measured at 600–800 °C in 3vol%H_2O-humidified H_2, with fits the model shown in (a). (c) Cross-sectional SEM image of the Ni–YSZ after testing. (d) Relative residuals between the EIS data and the fits, confirming the good fitting.

The EIS fitting was done using an ECM in Figure S14(a), aimed at enabling more accurate estimations of the ohmic resistance R_{Ω} and electrode polarization resistance R_{P}. The model, previously developed for the Ni–YSZ supported electrode symmetric cell [4–7], includes a simplified transmission line where R_{ion} and R_{rxn} represent oxygen vacancy transport within the YSZ phase of the Ni–YSZ electrode and the electrode/gas interfacial reaction, respectively. R_{Ω} models the ionic resistance of the electrolyte, while R_{HF} is associated with the grain boundary resistance in the YSZ phase of the Ni–YSZ electrode. W_{GFL} indicates a generalized finite length Warburg element for gas diffusion. Finally, L is included to account for inductive effects originating from the measurement circuit. The residuals, illustrated in Figure S14(d), all fall below ~1 %, indicating a good quality of fit.

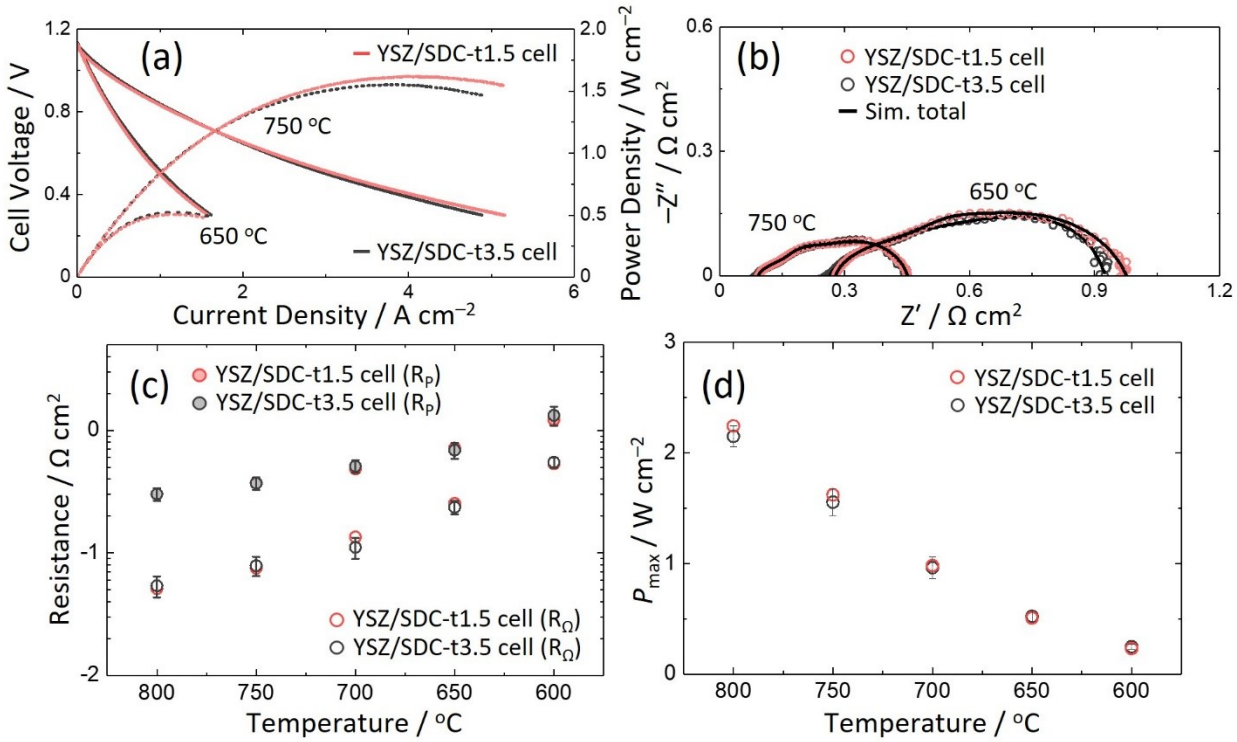

Fig. S15. (a) Cell voltage and power density versus current density, and (b) EIS data in Nyquist plots for Ni–YSZ FESCs with SDC layers of different thicknesses, *i.e.* 1.5 and 3.5 μm, measured in fuel cell mode at 650 and 750 °C. (c) Comparison of ohmic R_Ω and electrode polarization resistance R_P, and (d) peak power density across varying temperatures for both cells.

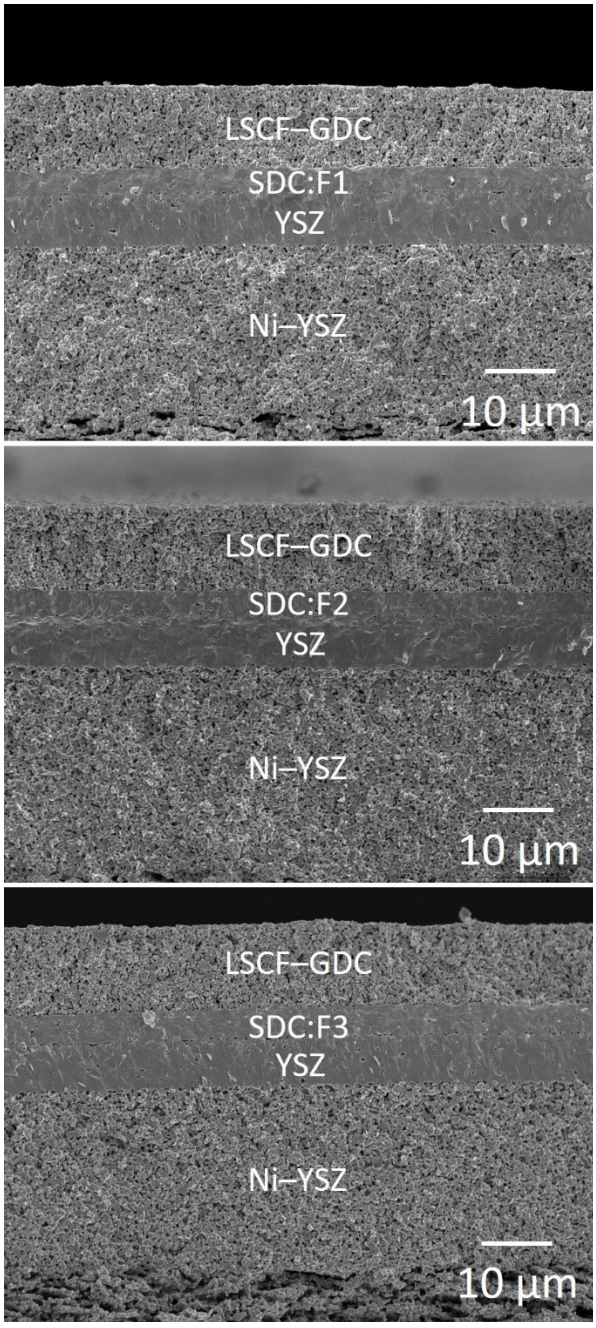

Fig. S16. Cross-sectional SEM images of the tested FESCs with YSZ/SDC:F1, YSZ/SDC:F2, and YSZ/SDC:F3 bi-layer electrolytes

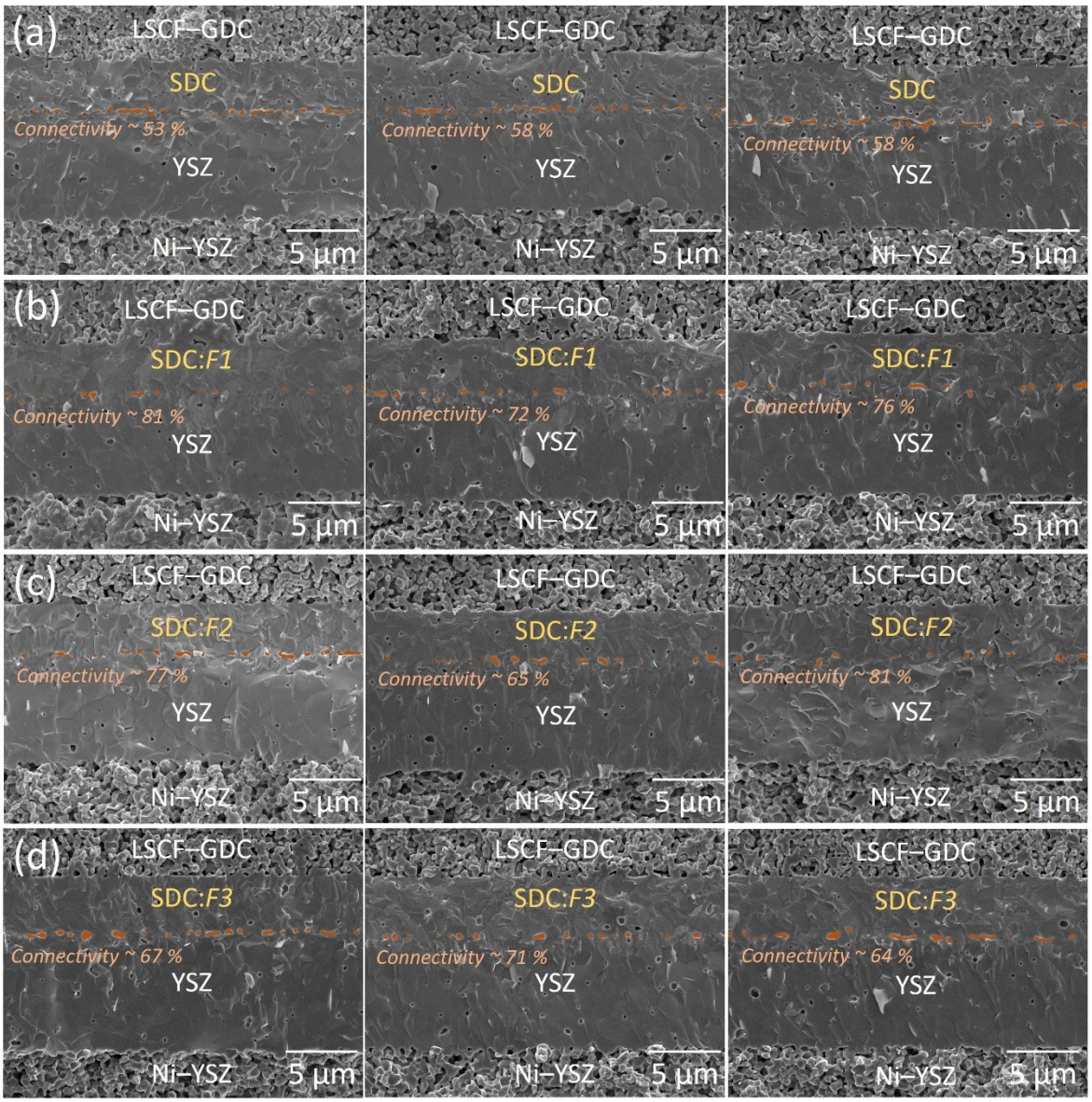

Fig. S17. Cross-sectional SEM images of the tested FESCs featuring (a) YSZ/SDC, (b) YSZ/SDC:F1, (c) YSZ/SDC:F2, and (d) YSZ/SDC:F3 bi-layer electrolytes, with the interfacial voids marked in red.

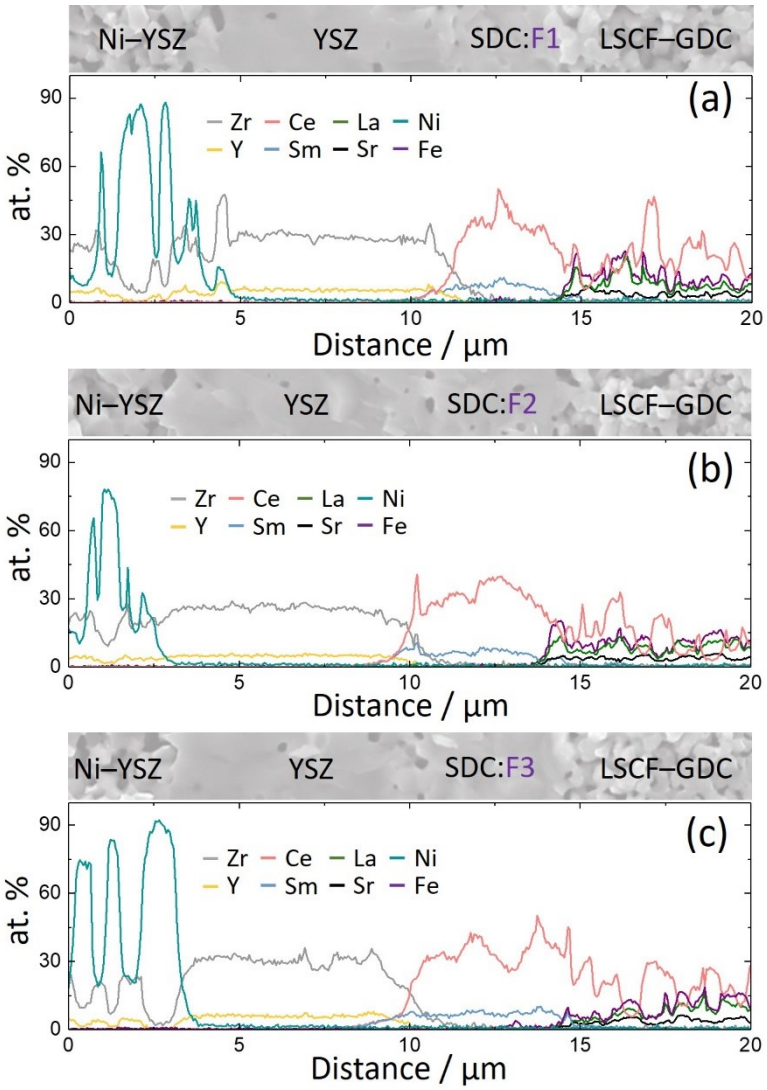

Fig. S18. SEM–EDS line scans illustrating the elemental distribution across the YSZ/SDC:F1, YSZ/SDC:F2, and YSZ/SDC:F3 bi-layer electrolytes.

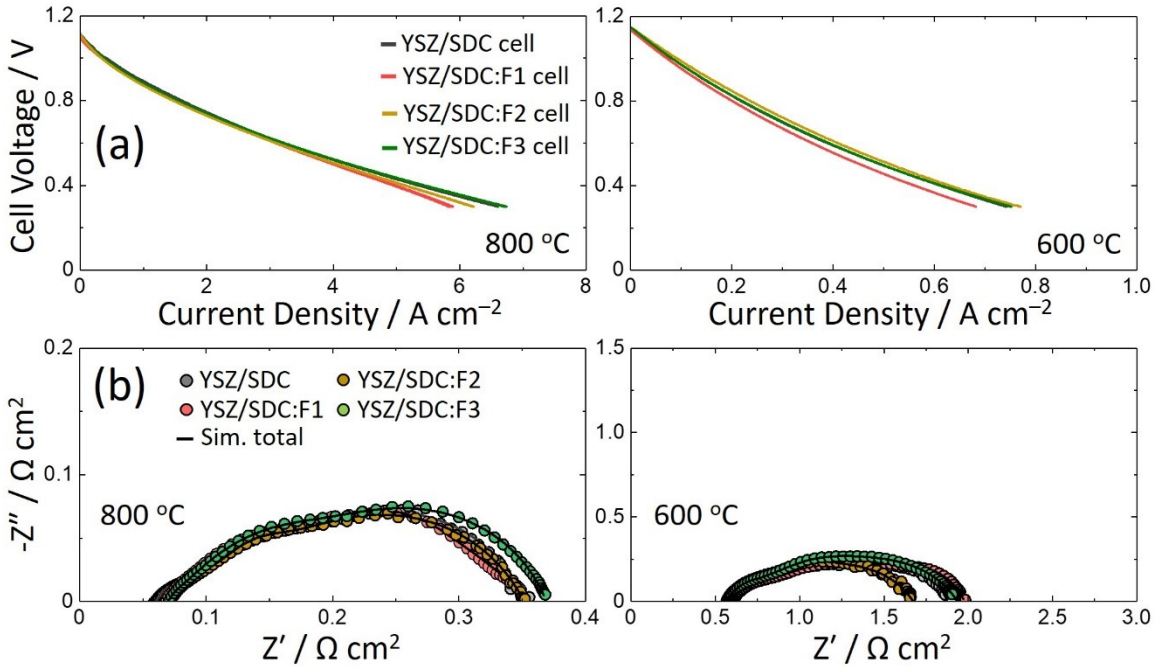

Fig. S19. (a) Cell voltage versus current density and (b) impedance spectra in Nyquist plots for full cells with YSZ/SDC, YSZ/SDC:F1, YSZ/SDC:F2, and YSZ/SDC:F3 bi-layer electrolytes, measured at 600 and 800 °C in 3 vol% H_2O-humidified H_2 and air.

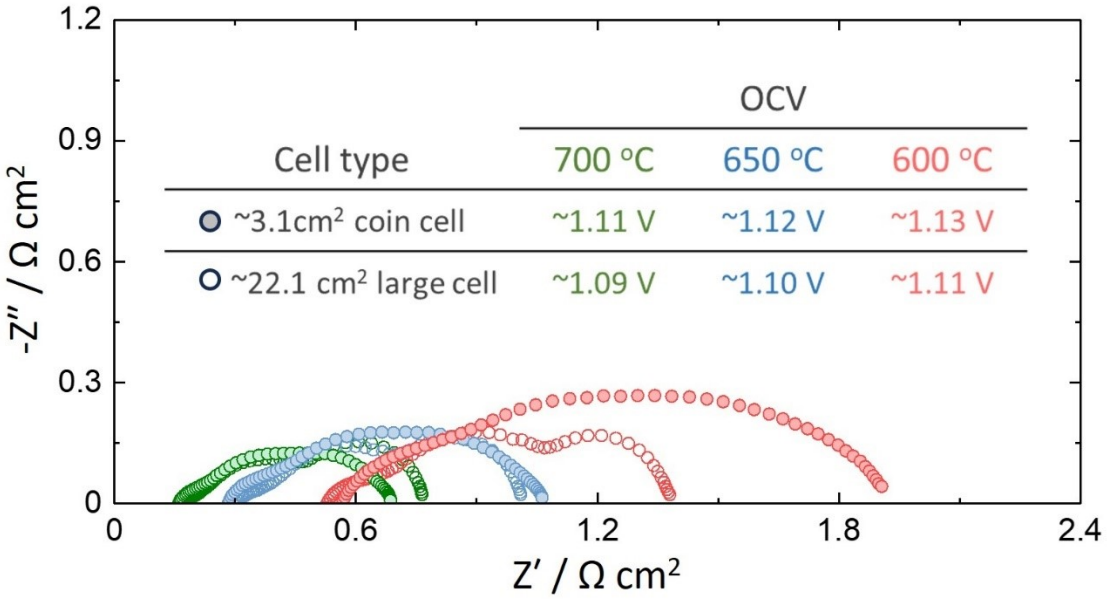

Fig. S20. Comparison of 600, 650 and 700 °C impedance spectra in Nyquist plots for the ~3.1 cm^2 coin cell with an ~0.5 cm^2 oxygen electrode and the ~22.1 cm^2 large cell with a 9 cm^2 oxygen electrode, where a YSZ/SDC:F1 bi-layer electrolyte is used in both.

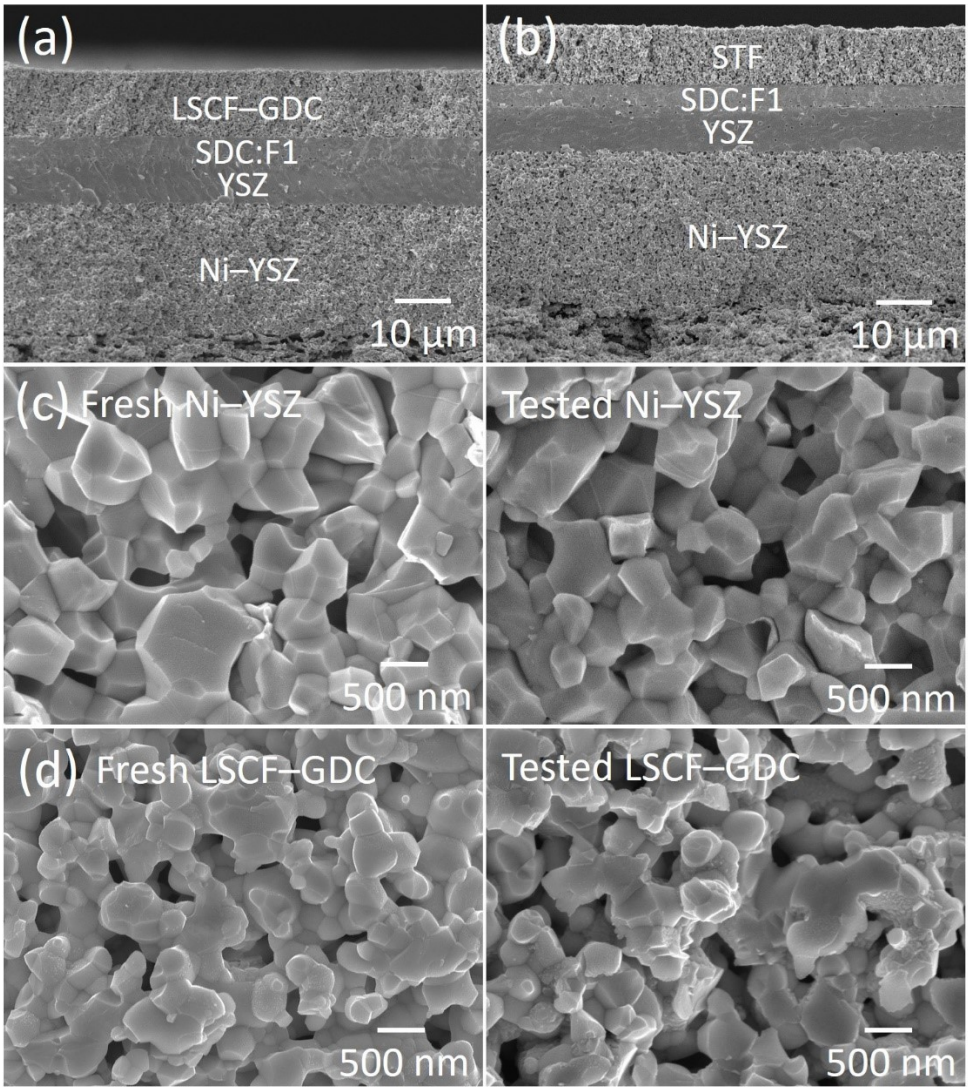

Fig. S21. Cross-sectional SEM images of YSZ/SDC:F1 bi-layer electrolyte-based full cells with different oxygen electrodes after 300 h of life testing at 800 °C fuel cell operation (3 vol% humidified H_2 and air) and j = 0.5 A cm^{-2}: (a) LSCF–GDC and (b) STF. SEM images of (c) the Ni–YSZ and (d) LSCF–GDC electrodes in the LSCF–GDC cell before and after the life test.

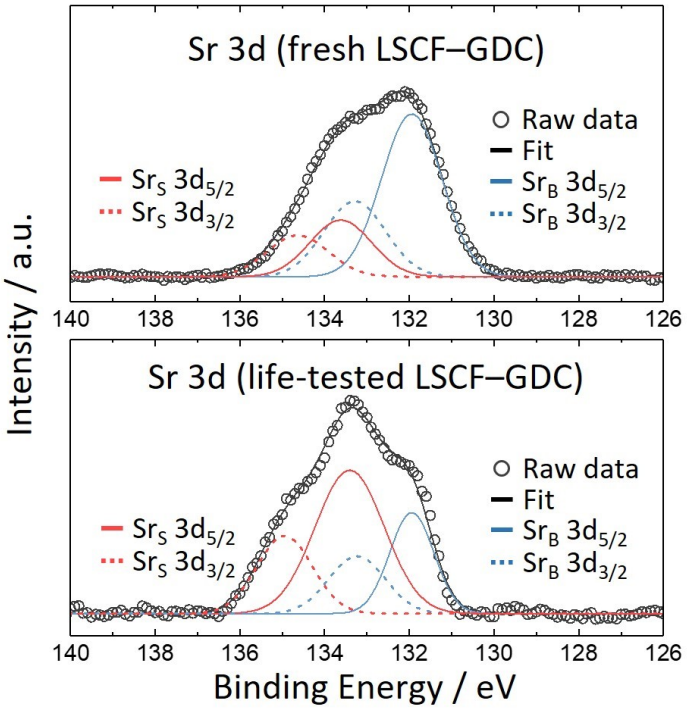

Fig. S22. XPS spectra of Sr 3d level and the peak fittings for fresh and life-tested LSCF–GDC oxygen electrodes.

The XPS surface composition analysis was done for LSCF–GDC oxygen electrodes of fresh and life-tested full cells. To confirm any surface-segregated Sr species, peak fitting was performed on the XPS spectra of the Sr 3d level, as shown in Figure S21. The analysis, coupled with data reported in previous literature [8-10], suggests the presence of both bulk-bound Sr and surface-bound Sr, each possessing a double state – $3d_{3/2}$ and $3d_{5/2}$. The pair with lower binding energy, ~133.5 eV for $3d_{3/2}$ and ~132 eV for $3d_{5/2}$ can be assigned to Sr in the LSCF perovskite oxide (Sr_B). On the other hand, the higher binding energy, ~135.5 eV for $3d_{3/2}$ and ~133.9 eV for $3d_{5/2}$ is attributed to surface Sr species, such as SrO, on the LSCF surface (Sr_S).

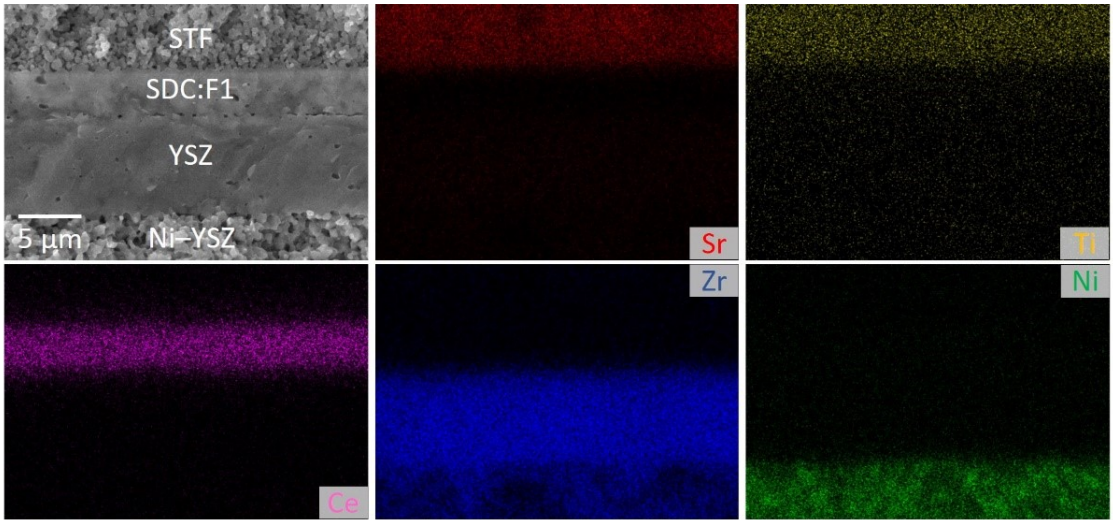

Fig. S23. Fracture cross-sectional SEM image along with EDS elemental maps for Sr, Ti, Ce, Zr, and Ni from the STF full cell after 300 h of life testing.

References

[1] J. Nielsen, T. Jacobsen, M. Wandel, Electrochim. Acta, 56 (2011) 7963.
[2] M.Y. Lu, R. Scipioni, B.-K. Park, T. Yang, Y.A. Chart, S.A. Barnett, Mater. Today Energy, 14 (2019) 100362.
[3] J. Ascolani-Yael, A. Montenegro-Hernández, Q. Liu, S.A. Barnett, L. Mogni, J. Electrochem. Soc., 166 (2019) F1301.
[4] J. Hong, A. Bhardwaj, Y. Namgung, H. Bae, S.-J. Song, J. Mater. Chem. A, 8, (2020) 23473.
[5] V. Sonn, A. Leonide, E. Ivers-Tiffée, J. Electrochem. Soc., 155 (2008) B675.
[6] B.-K. Park, R. Scipioni, D. Cox, S.A. Barnett, J. Mater. Chem. A, 8 (2020) 4099-4106.
[7] B.-K. Park, D. Cox, S.A. Barnett, Nano Lett., 21 (2021) 8363-8369.
[8] N. Ai, S. He, N. Li, Q. Zhang, W.D.A. Rickard, K. Chen, T. Zhang, S.P. Jiang, J. Power Sources, 384 (2018) 125-135.
[9] Y. Yu, K.F. Ludwig, J.C. Woicik, S. Gopalan, U.B. Pal, T.C. Kaspar, S.N. Basu, ACS Appl. Mater. Interfaces, 8 (2016) 26704-26711.
[10] Z. Pan, Q. Liu, L. Zhang, X. Zhang, S.H. Chan, J. Electrochem. Soc., 162 (2015) F1316.